PNAS RESEARCH ARTICLE | BIOCHEMISTRY

An integrated structural model of the DNA damage-responsive H3K4me3 binding WDR76:SPIN1 complex with the nucleosome

Xingyu Liu[a,1], Ying Zhang[a], Zhihui Wen[a], Yan Hao[a], Charles A.S. Banks[a], Joseph Cesare[a,b], Saikat Bhattacharya[a,2], Shreyas Arvindekar[c], Jeffrey J. Lange[a], Yixuan Xie[d,1], Benjamin A. Garcia[d,1], Brian D. Slaughter[a], Jay R. Unruh[a], Shruthi Viswanath[c], Laurence Florens[a], Jerry L. Workman[a], and Michael P. Washburn[a,3,4]

Affiliations are included on p. 11.

Edited by Ben E. Black, Perelman School of Medicine, University of Pennsylvania, Philadelphia, PA; received November 6, 2023; accepted June 21, 2024 by Editorial Board Member Karolin Luger

Serial capture affinity purification (SCAP) is a powerful method to isolate a specific protein complex. When combined with cross-linking mass spectrometry and computational approaches, one can build an integrated structural model of the isolated complex. Here, we applied SCAP to dissect a subpopulation of WDR76 in complex with SPIN1, a histone reader that recognizes trimethylated histone H3 lysine4 (H3K4me3). In contrast to a previous SCAP analysis of the SPIN1:SPINDOC complex, histones and the H3K4me3 mark were enriched with the WDR76:SPIN1 complex. Next, interaction network analysis of copurifying proteins and microscopy analysis revealed a potential role of the WDR76:SPIN1 complex in the DNA damage response. Since we detected 149 pairs of cross-links between WDR76, SPIN1, and histones, we then built an integrated structural model of the complex where SPIN1 recognized the H3K4me3 epigenetic mark while interacting with WDR76. Finally, we used the powerful Bayesian Integrative Modeling approach as implemented in the Integrative Modeling Platform to build a model of WDR76 and SPIN1 bound to the nucleosome.

chromatin | proteomics | integrated structural modeling | cross-linking mass spectrometry

The WD40 repeat containing protein, WDR76 (CMR1 or Ydl156w) was first identified in *Saccharomyces cerevisiae* as a histone-interacting protein (1). Affinity purification mass spectrometry (AP-MS) analyses of human WDR76 have identified a large number of intriguing protein interactions that alluded to distinct functions of WDR76 (2, 3) (Fig. 1*A*). Evidence from other studies also indicates the roles of WDR76 in diverse biological activities. Studies in different model organisms have discovered that WDR76 was involved in the DNA damage response (DDR) (1, 2, 4–7), transcriptional regulation (1, 8–10), and ubiquitination-based activities (11–15). Furthermore, key recent studies have demonstrated an important role of WDR76 in human disease (16) with specific studies demonstrating a role for WDR76 in both colon cancer (17, 18) and lung adenocarcinoma (19). A major challenge remains to determine the distinct protein complexes and interactions of WDR76 that control specific functions since it is unlikely that all legitimate interactions of WDR76 are functionally related in cells. To parse out the precise role of specific WDR76-containing complexes, we sought to isolate a subpopulation of these complexes and build an integrated structural model.

An important component of AP-MS identified WDR76 copurified proteins is the core histone subunits (1, 2) (Fig. 1*B*), indicating its involvement in chromatin related activities. Intriguingly, another WDR76 copurified protein, Spindlin-1 (SPIN1 or ORC) is also a histone binding protein. SPIN1 contains Tudor domains and has been shown to specifically bind H3K4me3 containing histone H3 peptide with high affinity (20–23). The interaction between WDR76 and SPIN1 is potentially significant to human health as SPIN1 is reported to promote cancer cell proliferation in multiple types of cancers (24–26). However, characterizing the complex of WDR76:SPIN1 and other coassociated proteins could be challenging using conventional AP-MS approaches. Key interactions of WDR76 and SPIN1 reported by others and our group were summarized in Fig. 1*A*. Among the most abundant WDR76 copurified proteins, the chromobox proteins (CBX1, CBX3, CBX5) (Fig. 1*B*) are not likely to be in the same complex with SPIN1 as they recognize opposite epigenetic markers (27–29). Likewise, SPINDOC (C11orf84), the most abundant interacting protein of SPIN1 (Fig. 1*B*), probably forms a different complex than SPIN1 forms with WDR76, as SPINDOC was not copurified with WDR76 (2, 3) and it prevents SPIN1 from binding H3K4me3 (30–32). Moreover, despite histone H3 being copurified with both WDR76 and SPIN1, there is insufficient evidence showing whether

Significance

In a regulated process that involves post-translational modifications on specific proteins called histones, different protein complexes will interact with histones organized into what is called the nucleosome. One such protein named Spindlin 1 interacts with an important histone posttranslational modification (PTM). The ability of Spindlin 1 to bind this specific histone PTM may be controlled by the other proteins Spindlin 1 interacts with. Here, we show that Spindlin1 can bind this important histone mark when Spindlin 1 is in complex with WDR76. In addition, using protein mass spectrometry and computational techniques we built a structural model of the Spindlin1 and WDR76 proteins with the nucleosome that provides insights into the function of these proteins.

The authors declare no competing interest.

This article is a PNAS Direct Submission. B.E.B. is a guest editor invited by the Editorial Board.

[1]Present address: Department of Biochemistry and Molecular Biophysics, Washington University St. Louis School of Medicine, St. Louis, MO 63110.

[2]Present address: Department of Biochemistry, University of Texas Southwestern Medical Center, Dallas, TX 75390.

[3]Present address: Department of Cancer Biology, University of Kansas Medical Center, Kansas City, KS 66160.

[4]To whom correspondence may be addressed. Email: mwashburn4@kumc.edu.

This article contains supporting information online at https://www.pnas.org/lookup/suppl/doi:10.1073/pnas.2318601121/-/DCSupplemental.

Published August 8, 2024.

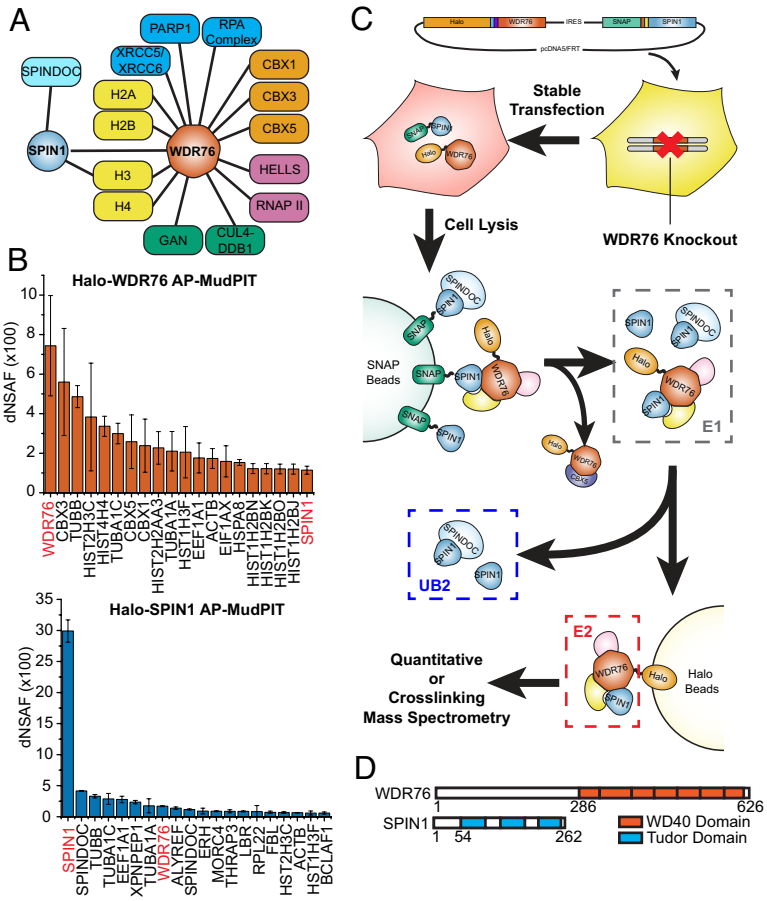

Fig. 1. Modified SCAP method to study WDR76 and SPIN1 containing protein complex. (*A*) Selected potential interacting proteins of WDR76 and SPIN1 identified by AP-MS. (*B*) MudPIT analysis of WDR76 copurified and SPIN1 copurified proteins. Top 20 proteins ranked by dNSAF values in Halo-WDR76 (*Left*) or Halo-SPIN1 (*Right*) purification are showed. Each dNSAF value plotted is the average from three biological replicates; error bars represent SD. (*C*) Schema of using SCAP method to investigate cointeracting proteins of WDR76 and SPIN1. The modified SCAP pipeline started with generating the stable cell line expressing tagged bait proteins in absent of endogenous version of the second bait protein (WDR76 in this example), and then this cell line was used to provide material for SNAP purification followed by Halo purification. Samples might be analyzed by quantitative mass spectrometry (SCAP-MS) or be subjected to cross-linking steps (SCAP-XL). (*D*) Domain map of WDR76 and SPIN1.

they interact with H3 as a complex or these are independent interacting partners. To this point, purification methods that effectively enrich a specific subset of interactions are keenly needed to characterize the assemblies formed by proteins engaged in multiple complexes, like WDR76 and SPIN1.

We have previously described the Serial Capture Affinity Purification (SCAP) approach, in which a combination of two separately tagged bait proteins, Halo-tagged SPIN1 and SNAP-tagged SPINDOC, were coexpressed and purified in sequence to reduce the complexity of purified samples (32). In the same study, we demonstrated the striking capability of the SCAP system in obtaining highly purified and enriched SPIN1:SPINDOC complexes and used the extended cross-linking analysis pipeline, SCAP-XL, in integrative structural modeling (32). The SCAP method can be used to isolate specific complexes of proteins that function in multiple distinct assemblies by sequentially affinity purifying two distinctly affinity-tagged bait proteins.

Here, we show the ability of the SCAP approach to isolate WDR76:SPIN1:Nucleosome complexes using Halo-WDR76 and SNAP-SPIN1 as bait proteins (Fig. 1*C*). We first coexpressed bait proteins in cells depleted of endogenous WDR76. Using the modified SCAP-MS and SCAP-XL pipelines, we separated the WDR76:SPIN1 complex from other WDR76 complexes containing CBX proteins and the SPIN1:SPINDOC complexes. We demonstrate the potential for both SPIN1 and WDR76 to respond to DNA Damage. Multiple distinct cross-links were found between WDR76, SPIN1, and histones from the cross-linking mass spectrometry (XL-MS) analysis of SCAP-purified complexes. An initial integrative structural model demonstrated that SPIN1 in complex with SPINDOC did not interact with histones and blocked the ability of SPIN1 to bind H3K4me3 (32). Here, in contrast, the WDR76:SPIN1 complex interacted with histones and SPIN1 was able to bind H3K4me3. Finally, given the 149 pairs of cross-links identified between SPIN1, WDR76, and histones, we then performed Bayesian integrative modeling as implemented in the Integrative Modeling Platform (IMP) (33–36) to build an integrative structural model of WDR76 and SPIN1 docked onto the nucleosome.

Results

Analysis of WDR76 and SPIN1 Single-Bait AP-MS. We first analyzed interactions of WDR76 and SPIN1 separately using Halo-tag AP-MS. Our updated WDR76 AP-MS results are mostly consistent with previous data (2, 3). In this experiment, we identified 395 proteins significantly enriched over control purifications (Dataset S2A). Among the top 20 proteins ranked by abundance, we detected histones (H2A, H2B, H3, and H4), CBX proteins (CBX1, CBX3, and CBX5), and SPIN1 (Fig. 1*B*). Members of the chaperonin containing TCP1 complex (CCT or TriC complex) were the next abundant proteins enriched in the list. We also detected other previously reported interactions, such as HELLS, SIRT1,

HDAC1, HDAC2, and proteins involved in DNA damage repair (XRCC5, XRCC6, PARP1, PRKDC, DDB1, RAD23B) (2, 3). In agreement with a published data which suggested a role of WDR76 in targeting proteins for ubiquitination and degradation (11–15), we recovered several ubiquitination related proteins including DCAF7, USP7, USP11, USP9X, HUWE1, and UBR5. Taken together, these data alongside previous reports highlight the diverse protein interaction networks associated with WDR76.

In our new AP-MS data of SPIN1, we found more copurified proteins than prior experiments (32). A total of 292 proteins were significantly enriched (Dataset S2A). SPINDOC was the most abundant protein other than the bait protein, SPIN1 (Fig. 1*B*). WDR76 was also among the most abundant proteins with an average dNSAF value of 0.017. Other interesting proteins in the top 20 most abundant proteins included histone H3, lamin-B receptor that links chromatin to nuclear envelope (37) and several mRNA processing and export related proteins (ALYREF, THRAP3, BCLAF1, ERH) (Fig. 1*B*). In addition, proteins involved in histone methyltransferase complexes (KMT2A, KMT2B, RBBP5, DPY30, ASH2L, PRMT1, FBL, MEN1) and cell cycle related proteins (MCM proteins and RPA proteins) copurified with Halo-SPIN1 (Dataset S2A). However, no functional implication of SPIN1 and WDR76 together became apparent by comparing their single-bait AP-MS results.

Observing that core histone H3 was identified as a top copurified protein in both WDR76 and SPIN1 purifications (Fig. 1*B* and Dataset S2A), we proposed that the unique histone marks enriched by these two proteins of interest could be key indicators of their collaborative function. A comprehensive analysis of post-translational modifications (PTMs) on histones copurified with WDR76 or SPIN1 by Halo-AP was performed (Dataset S3). By comparing to the total histones extracted from the corresponding cell line used as input for purification, several PTMs were found significantly enriched in SPIN1 or WDR76 (*SI Appendix*, Fig. S1 and Dataset S3C). Many histone marks typically associated with transcriptionally active sites, such as methylated H3K4, H3K9ac, and H3K27ac, were significantly enriched in histones copurified with SPIN1(*SI Appendix*, Fig. S1). Particularly, H3K4me3 was enriched 128-fold by SPIN1 pulldown. This result is consistent with previous studies demonstrating that SPIN1 specifically recognizes H3K4me3 via its Tudor domains (22, 23). Conversely, although H3K4me3 and H3K9ac were also copurified with WDR76, their enrichment in the WDR76-associated histones was not as pronounced as for SPIN1 (around threefold for H3K4me3 and twofold for H3K9ac) (*SI Appendix*, Fig. S1). Considering our AP-MS results, which showed that WDR76 pulls down proteins known to bind different histone marks (Fig. 1 *A* and *B*), this observation is reasonable assuming that only a subpopulation of WDR76 would enrich for these marks. Thus far, our proteome and histone PTM analysis on WDR76 and SPIN1 APs together have indicated the potential formation of a complex by WDR76 and SPIN1 capable of binding H3K4me3. Therefore, we implemented the SCAP approach to gain more insight into the function of the specific WDR76:SPIN1 subcomplex.

In Vivo Interaction between WDR76 and SPIN1. The Halo tag (38) and SNAP tag (39) have been selected as the affinity tags in SCAP, which allows for convenient differential imaging of the bait proteins. Before applying SCAP to purify WDR76 and SPIN1, we took advantage of the imaging feature to validate the interaction between Halo-WDR76 and SNAP-SPIN1 in live cells using acceptor photobleaching Förster resonance energy transfer (apFRET) assay (40) and fluorescence cross-correlation spectroscopy (FCCS) assay (41). Similar to assessing SPIN1 and SPINDOC by Liu et al. (32), Halo-WDR76 and SNAP-SPIN1 were coexpressed, stained with the corresponding fluorescent ligands, and imaged in live cells (*SI Appendix*, Fig. S2). In the apFRET assay (*SI Appendix*, Fig. S2 *A–C*), we observed about 2% of FRET efficiency between Halo-WDR76 and SNAP-SPIN1, which was significantly higher than that measured with SNAP-Control (*SI Appendix*, Fig. S2*B*). In the FCCS assay, we observed a cross-correlation of Halo-WDR76 and SNAP-SPIN1 but not Halo-WDR76 and SNAP-Control (*SI Appendix*, Fig. S2*D*). The fraction of Halo-WDR76 binding to SNAP-SPIN1 was also calculated using y amplitudes of self- and cross-correlation curves (*SI Appendix*, Fig. S2*E*). In summary, the positive FRET result indicated a direct interaction of WDR76 and SPIN1 in vivo and the FCCS result suggested WDR76 and SPIN1 codiffuse in a complex. The FCCS result was particularly intriguing because it also suggested that the complex formed by WDR76 and SPIN1 is mobile in the nucleus. As we mentioned above, both WDR76 and SPIN1 may interact with core histones (Fig. 1*B* and Dataset S2A). Moreover, chromatin immunoprecipitation assays have indicated that both WDR76 (10) and SPIN1 (25) bind to chromatin. Since chromatin associated species are usually less mobile and difficult to measure by FCCS, our result indicated that WDR76 and SPIN1 might form a complex independent of their binding to chromatin. This result also raised the question whether WDR76:SPIN1 in complex would bind to histones although histone H3 was enriched in both WDR76 and SPIN1 purifications (Fig. 1*B*).

SCAP Analysis of WDR76 and SPIN1. In the formerly described SCAP workflow, we generated cell lines stably expressing both bait proteins using a dual-expression plasmid from wildtype parental cells, in which the endogenous bait proteins remain present (32). Using the stable-expressing cells, proteins from whole cell extracts were first isolated on SNAP affinity beads and then eluted using PreScission protease to obtain fraction E1. Then, E1 was purified in tandem using Halo affinity beads. The unbound supernatant of the Halo purification was collected as fraction UB2. The proteins captured by the Halo beads were eluted using the TEV protease as fraction E2. One major concern of using such cell lines to perform SCAP is the competition from the endogenous version of the bait protein for the later purification step. These untagged proteins might be captured with the SNAP-tagged bait but cannot be captured during Halo purification; thus, a portion of coassociated proteins would be lost in the final fraction E2. Though the original SCAP protocol still functioned for SPIN1 and SPINDOC (32), removing untagged version of the Halo bait protein from the system should theoretically enhance the yield of SCAP. For WDR76 and SPIN1, we first depleted the endogenous WDR76 (the Halo-tagged bait for the second purification in SCAP) from HEK293 cells bearing a FRT recombination site by deleting both alleles of the corresponding gene, and then, we built cell line expressing Halo-WDR76 and SNAP-SPIN1 in this WDR76 knockout background (Fig. 1*C*). Using these cells, the WDR76 captured in E1 were completely tagged by Halo and enriched by serial capture. In addition, we optimized several steps of the SCAP protocol: We tripled the number of cells to extract proteins at a higher yield; we subjected 90% of E1 to subsequent purification to use more material in the final enrichment; we also adjusted conditions and timing of purification steps. Comparable amount of E1, UB2, and E2 samples from each SCAP experiment were analyzed with label-free quantitative proteomics (SCAP-MS), multidimensional protein identification technology (MudPIT) (42) (Dataset S2B and *SI Appendix*, Fig. S3). The modified SCAP-MS workflow is demonstrated in Fig. 2*A*. For a better comparison of SCAP-MS and single-bait AP-MS of WDR76, we also generated

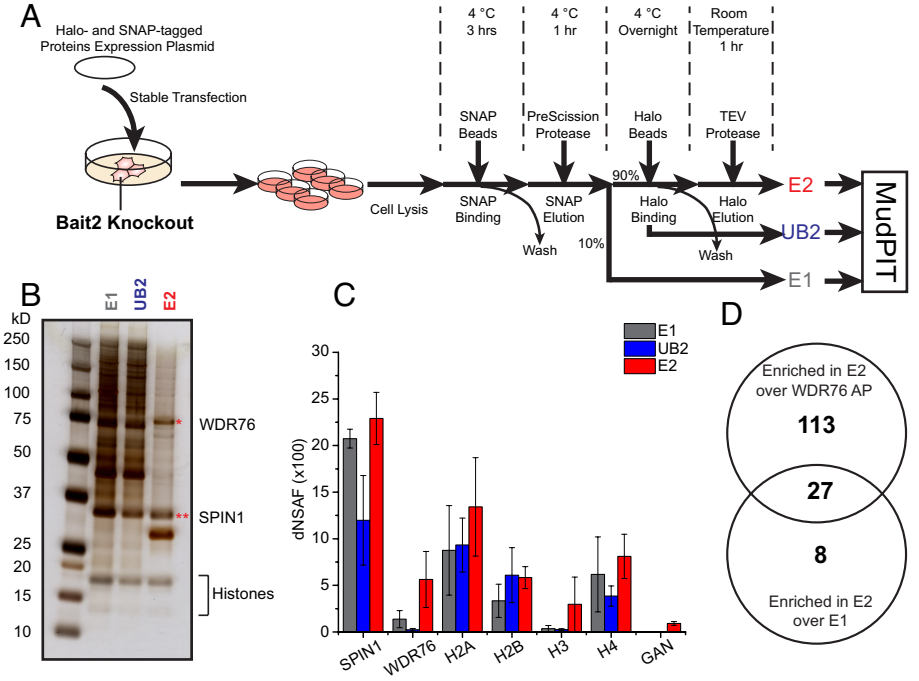

Fig. 2. Analyzing copurified proteins of WDR76 and SPIN1 with a modified SCAP workflow followed by MudPIT. (*A*) A modified workflow of SCAP followed by quantitative proteomics analysis (SCAP-MS). For obtaining materials for SCAP, stable transfection of the dual-expression vector is performed on cells deleted of the endogenous bait protein in the second step of purification (Bait2). SCAP purification is similar to the original workflow (32) with minor optimization. E1, UB2, and E2 fractions were all separately analyzed by MudPIT and dNSAF values were calculated from spectra counts for all identified proteins. (*B*) Silver stained SDS-PAGE of the proteins in the E1, UB2, and E2 fractions of SCAP using Halo-WDR76 and SNAP-SPIN1 as bait proteins. The anticipated band of WDR76 is marked with * and SPIN1 is marked with ** based on their sizes. Bands of histones are expected to appear in the range below 20 kD. (*C*) The dNSAF values of WDR76, SPIN1, GAN, and histones in E1, UB2, and E2 fractions. Each dNSAF value plotted is the average from three biological replicates; error bars represent SD. (*D*) Venn diagram showing numbers of proteins enriched in E2 fraction over E1 and enriched by SCAP over single-bait WDR76 purification. There are 27 proteins shared by both groups of enriched proteins.

a stable cell line that expresses Halo-WDR76 alone in the same WDR76 knockout background to perform AP-MS (Dataset S2C).

The modified SCAP method again showed the striking capability to reduce sample complexity (Fig. 2*B*), illustrated by a much cleaner E2 sample compared to E1. In this SCAP-MS analysis of WDR76 and SPIN1, we detected in total 699 proteins in at least one of E1 or E2 fraction and 165 proteins in E2 were significantly enriched over the blank control purification (Dataset S2 B and F). The top 20 proteins ranked by dNSAF values in E2 are shown in *SI Appendix*, Fig. S3*C*. Besides the high abundance of both bait proteins in E2, other proteins, including histones and GAN, were also among the top 20 identifications, suggesting their strong association with both WDR76 and SPIN1. Upon comparing the three fractions, WDR76, GAN, and histones appeared more abundant in E2 than E1 (Fig. 2*C*). By comparing E1 and E2 statistically using QSPEC (43), WDR76, GAN, histone H2A, H2B, and H3 were significantly enriched in E2 over E1 (Dataset S2 B and F). The other bait SPIN1 was not further enriched during the 2nd purification step (Fig. 2*C*), which could be explained by only a fraction of SPIN1 was bound by WDR76 in cells. In addition to the most abundant detections, we also identified other cocaptured proteins of WDR76 and SPIN1 in E2, which might also provide clues for the functions of the complex. Among the 165 proteins enriched in E2 over control, 35 proteins were significantly enriched in E2 over E1 and 140 over single-bait Halo-WDR76 copurified samples (Dataset S2 C and F). Binary analysis of the 35 and 140 proteins found 27 proteins of overlap, which were enriched in E2 over both E1 and WDR76 purification (Fig. 2*D* and Dataset S2F). As expected, the CBX proteins were no longer significantly enriched by SCAP compared to Halo-WDR76 purification alone, demonstrating that the SCAP method can distinguish a subpopulation of WDR76 molecules in complex with SPIN1.

The major components in E2, including SPIN1, WDR76, all four canonical histones (H2A, H2B, H3, H4) and GAN, constituted about 60% of the total sample (summed average dNSAF value: 0.598). This enrichment was similar in the SCAP-MS analysis of SPIN1 and SPINDOC, in which SPIN1:SPINDOC complex was also about 60% of total proteins in E2 (32). Intriguingly, taken together the SCAP-MS results of Halo-WDR76/SNAP-SPIN1 and Halo-SPIN1/SNAP-SPINDOC (32) also suggested that SCAP method successfully distinguished two SPIN1-containing protein complexes (Dataset S2D). When comparing to the single-bait Halo-SPIN1 purification, WDR76 was significantly enriched by SCAP using both Halo-WDR76 and SNAP-SPIN1 as baits, indicating the successful purification of WDR76:SPIN1 over other SPIN1 interactions. In contrast, the SPINDOC protein copurified with SNAP:SPIN1 in E1 was barely captured during the second step of WDR76:SPIN1 SCAP (dNSAF in E2: 0.005) compared to unbound fraction UB2 (*SI Appendix*, Fig. S3). In the SPIN1:SPINDOC SCAP-MS analysis, we published previously (32), WDR76 was not detected in E2 at all (Dataset S2D). These results suggest that SPIN1 forms distinct protein complexes with SPINDOC and WDR76.

SPIN1 binds H3K4me3 (20, 22, 23) and various histones were identified in WDR76 AP-MS analyses (1–3). In agreement with published results, the single-bait AP-MS data in this study showed that WDR76 copurified with all four types of core histones while SPIN1 mostly copurified histone H3 (Fig. 3*A* and Dataset S2 A–C). In the SCAP-MS analysis of WDR76:SPIN1, core histones (H2A, H2B, H3, and H4) were also among the most abundant proteins cocaptured with WDR76:SPIN1 (Fig. 2*C* and Dataset S2B). In addition, Histone H2A, H2B, and H3 were among the 27

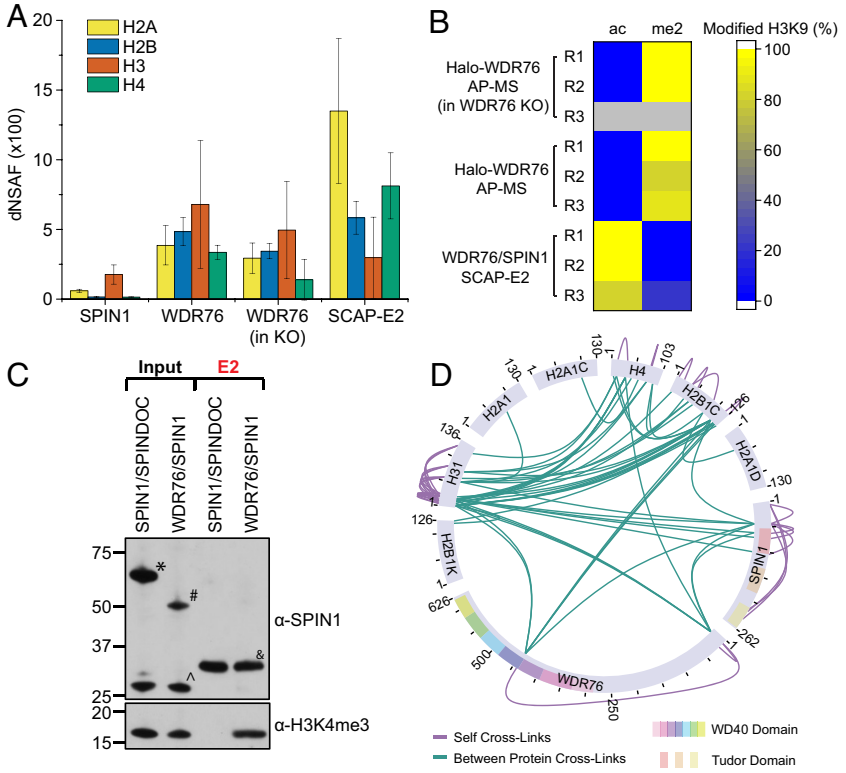

Fig. 3. Characterizing the interactions between the WDR76:SPIN1 protein complex and different types of core histones with SCAP-MS and SCAP-XL. (*A*) The dNSAF values of core histones in samples obtained from different purifications. All single-bait purifications were Halo purifications. Halo-WDR76 purification was performed either with or without the present of endogenous WDR76. SNAP-SPIN1 and Halo-WDR76 were baits for SCAP. Each dNSAF value plotted is the average from three biological replicates; error bars represent SD. (*B*) Distinct PTM status of H3K9 on histone H3 captured in SCAP E2 fraction versus that of histone H3 captured in single-bait purification using WDR76 as bait. The percentages of modified H3K9 were calculated from spectral counts. Three replicates for each type of experiment are shown. (*C*) Comparison of lysine four trimethylated histone H3 copurified with WDR76:SPIN1 or SPIN1:SPINDOC complex by SCAP. The shared bait protein, SPIN1, was detected by antibodies that recognize both endogenous and tagged versions of SPIN1. SCAP purification was performed from extracts of 293FRT cells expressing SNAP-Flag-SPIN1 + Halo-HA-WDR76 and Halo-HA-SPIN1 + SNAP-Flag-SPINDOC. Input and eluted fractions were resolved on gels followed by silver staining and western blotting. The expected band for Halo-HA-SPIN1 is represented by asterisk (*), for SNAP-Flag-SPIN1 is represented by hash (#), for the endogenous SPIN1 is represented by circumflex (^), and for the eluted HA or Flag-SPIN1 is represented by the ampersand (&). This result was validated by two other repeated sets of purifications. (*D*) Direct interactions between WDR76, SPIN1, and various types of histones revealed by SCAP coupled with cross-linking mass spectrometry analysis (SCAP-XL). The cross-links were visualized in circle view generated with xiView (44).

proteins more enriched in E2 over both E1 and WDR76 purification (Dataset S2F). These results suggested that WDR76 and SPIN1, when forming a complex, were still able to interact with histones. Since the complex copurified with all four types of histones as WDR76 but SPIN1 alone captured less histone H2A, H2B, and H4 (Fig. 3*A*), the binding of SPIN1 to WDR76 did not disrupt the interactions of WDR76 with histones. Furthermore, since other WDR76 copurified proteins, the CBX proteins (Fig. 1*B*), recognize opposite post translational modifications (PTMs) on histone H3 from SPIN1 (27–29), we raised the possibility that WDR76 might interact with differently modified histones when associated with different histone PTM readers. With the AP-MS and SCAP-MS data above, we were able to analyze the PTMs on H3K9 (Dataset S2E). As shown in Fig. 3*B*, high levels of acetylation on H3K9, which is also considered a transcriptionally active modification that sometimes coexist with H3K4me3, were detected in the E2 fraction of WDR76:SPIN1 SCAP, but not in single-bait WDR76 purifications. While trimethylation levels on H3K4 could not be measured due to this short peptide being difficult to identify by LC/MS, we tested the presence of H3K4me3 in proteins copurified with WDR76:SPIN1 by Western blot analysis (Fig. 3*C*). We assessed H3K4me3 levels in both SPIN1:SPINDOC and WDR76:SPIN1. As shown in Fig. 3*C*, H3K4me3 was clearly copurified with WDR76/SPIN1 but was absent for SPIN1:SPINDOC. This observation is consistent with our previous conclusion that the binding of SPINDOC to SPIN1 could interrupt the binding of SPIN1 to H3K4me3 (32). Taken together, the WDR76:SPIN1 complex prefers to bind histone H3 bearing specific PTMs, and this selectively is likely mediated by SPIN1.

The WDR76:SPIN1 Complex Directly Interacts with Histones. To identify direct interactions and to gain structural insights into the WDR76:SPIN1 complex, we next implemented SCAP-XL, where we first performed the modified SCAP for Halo-WDR76 and SNAP-SPIN1 followed by cross-linking reaction on samples using a MS-cleavable cross-linker, DSSO (disuccinimidyl sulfoxide) (*SI Appendix*, Fig. S4*A*). Then, we analyzed cross-linked E2 fraction by cross-linking mass spectrometry (XL-MS) and visualized the data using xiVIEW (44) (Dataset S4A). Detected cross-links to WDR76, SPIN1, and histones are shown in circular view (Fig. 3*D*). WDR76 and SPIN1 were cross-linked to each other, which confirmed their direct interaction as we also proved by an apFRET assay (*SI Appendix*, Fig. S2*B*). Histone H2B, H3, and H4 from the list of top identifications in SCAP-MS were also cross-linked to one or both baits, suggesting that WDR76 and SPIN1 directly interact with these histones. Histone H2B and H3 were found to cross-link to WDR76 and SPIN1 with multiple cross-links, while H4 was only cross-linked to WDR76 with one cross-link. Histone H2A, despite its high abundance in cocaptured proteins of WDR76 and SPIN1 (Fig. 2*C*), was not found directly cross-linked to either bait.

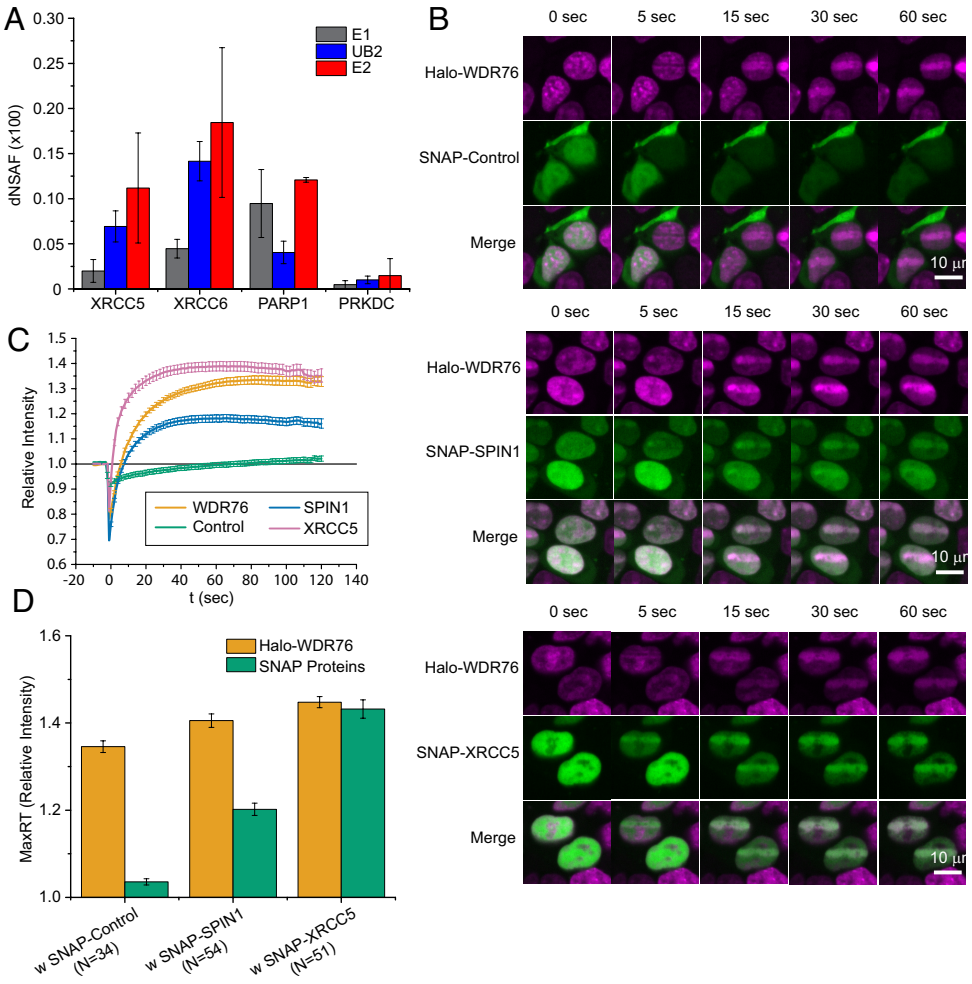

Fig. 4. Potential function of WDR76:SPIN1 complex in DDR. (*A*) Identification of proteins involved in NHEJ. Each dNSAF value plotted is the average from three biological replicates; error bars represent SD. (*B*) Examples of time course imaging. In each experiment, a SNAP-tagged protein was coexpressed with Halo-WDR76. Halo-tagged proteins were labeled with HaloTag TMRDirect ligands and SNAP-tagged proteins were labeled with SNAP-Cell 505-Star ligands. Cells were also stained with HOECHST 33258. Further, 405 nm UV laser damage was introduced at timepoint 0 in a stripe-shaped confined area. (*C*) Recruitment of Halo- or SNAP-tagged proteins to laser induced damages. Recruitment level is presented by relative intensity at the stripe, calculated from the intensity of each timepoint normalized to the intensity before microirradiation. For Halo-WDR76, the sample coexpressed with SNAP-Control is plotted. Each data point is an average from all measured cells; error bars stand for SEM. (*D*) The maximum recruitment of each protein within 2 min after microirradiation. Each maximum recruitment value is an average from all measured cells; error bars stand for SEM.

However, cross-links were detected between histones, thus H2A likely interacted with the WDR76:SPIN1 complex indirectly as part of the nucleosome. Histone H3 was cross-linked to WDR76 and SPIN1 with its N-terminal region, in contrast, H2B was cross-linked to the baits through its C terminal region. Cross-linking sites distributed mostly near the SPIN1 N-terminal region, while no cross-linking site fell in the second Tudor domain, where the pocket to bind H3K4me3 is located (22, 23). In contrast to the SCAP-XL result, the XL-MS analysis of Halo-WDR76 single bait purification did not identify cross-linked peptides from SPIN1 (*SI Appendix*, Fig. S4*C* and Dataset S4D). Histone H2B, H3, and H4 were cross-linked to WDR76, however, only H3 was detected with more than one cross-link (*SI Appendix*, Fig. S4*C*).

Next, we performed structural modeling for tridimensional visualization of cross-links. Although several crystal structures of SPIN1 have been published (21–23), the N-terminal region, where some critical cross-linked lysine residues reside, was not covered by these structures. Since the structures of both full-length WDR76 and SPIN1 are not available, we performed ab initio prediction of their structures with I-Tasser (45, 46) from amino acid sequences. I-Tasser provided five models for each protein. Intra-crosslinks were mapped to the predicted models (*SI Appendix*, Fig. S5 *A* and *B*) and distances between crosslinked residues were measured (Dataset S5A). For WDR76, we obtained two properly folded models, model3 and model5, and 5 out of 6 detected intra-cross-links could be satisfied in both models (*SI Appendix*, Fig. S4*A*). For SPIN1, models were more similar to each other (*SI Appendix*, Fig. S5*B*). Model2 matched all intra-SPIN1 cross-links (Dataset S5A) and therefore was selected as our best model for docking with WDR76. This model can also be largely aligned to a known SPIN1 structure in PDB: 4mzf (23) (*SI Appendix*, Fig. S5*C*). After filtering inter-cross-links between WDR76 and SPIN1 with DisVis (47, 48) (Dataset S5B), we chose WDR76 model3 to dock with SPIN1 model2. The docking was performed with HADDOCK 2.4 webserver (49, 50) using the three inter-cross-links between WDR76 and SPIN1 as restraints (Dataset S5C). The best four models from the top cluster with the lowest HADDOCK score are shown in ensembled representation (*SI Appendix*, Fig. S6*A*). Cross-links were mapped to these models and the distance restraints were all satisfied by four models (Dataset S5D). The model with the lowest energy was used as an example for visualization (*SI Appendix*, Fig. S6 *B* and *C*). From *SI Appendix*, Fig. S6*B*, we noticed that the interface between WDR76 and SPIN1 in this model did not overlap with the Tudor

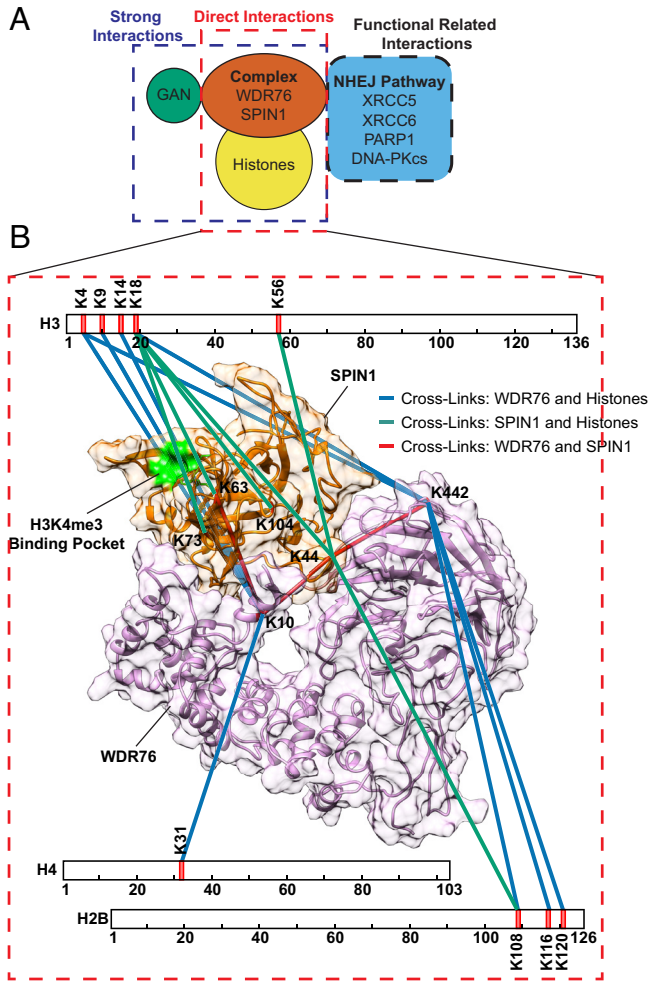

Fig. 5. Model of SCAP-MS and SCAP-XL results using Halo-WDR76 and SNAP-SPIN1 as bait proteins. (*A*) From the quantitative analysis of SCAP samples, GAN and core histones were identified as strong interactions of WDR76:SPIN1 complex based on their abundance in E2 fraction. Low abundant interactors, including XRCC5, XRCC6, DNA-PKcs, and PARP1, indicated the potential roles of both WDR76 and SPIN1 in DNA damage response. DSSO cross-linking of SCAP-purified proteins followed by mass spectrometry analysis further supported the direct physical interaction between WDR76 and SPIN1. Cross-links between WDR76:SPIN1 and histones also suggested direct protein–protein interactions. (*B*) Visualization of direct cross-links to WDR76 or SPIN1. WDR76:SPIN1 complex is displayed by a predicted structural model in surface view, in which WDR76 is colored in plum color and SPIN1 is colored in orange. The H3K4me3 binding pocket of SPIN1 is colored in green. All cross-linked lysine residues were labeled and marked in red. Cross-links between WDR76 and SPIN1 are shown as red lines. Cross-links between histones and WDR76 are shown as blue lines, while those between histones and SPIN1 are shown as green lines.

domains of SPIN1. Then, we aligned the WDR76:SPIN1 model to a known SPIN1 structure containing a methylated histone H3 peptide (PDB: 4mzf) (23) in *SI Appendix*, Fig. S6*C* to check whether WDR76 would interfere with the binding of SPIN1 to H3. The histone H3K4me3R8me2a binding pocket of SPIN1 indicated by Su et al. (23) was not occluded by WDR76 in the complex model (*SI Appendix*, Fig. S7*A*). In contrast, this binding pocket was occluded in the SPIN1:SPINDOC complex model (*SI Appendix*, Fig. S7*B*).

Function of WDR76:SPIN1 in the DNA Damage Response. Besides histones, SCAP-MS analysis of WDR76 and SPIN1 identified other less abundant cocaptured proteins enriched in E2. Noticeably, both XRCC5 and XRCC6 were among the 27 proteins more enriched in E2 over both E1 and WDR76 single-bait purification (Dataset S2E). XRCC5 and XRCC6 form as a heterodimer (Ku complex) that binds double-strand DNA. A well-known function of the XRCC5/XRCC6 dimer is that it is recruited to DNA double-strand breaks in the Non-Homologous DNA End Joining (NHEJ) pathway (51). Other proteins involved in the NHEJ pathway, DNA-PKcs (PRKDC), and PARP1, were also identified by SCAP-MS (Fig. 4*A*). This result strongly implied a potential function of the WDR76:SPIN1 complex in NHEJ. WDR76 has been reported to be involved in DDR and factors in NHEJ repair pathway were identified by WDR76 AP-MS (2–7). SPIN1, however, has never been linked to DDR in existing data, besides its interaction with WDR76. Our data showed that XRCC5/XRCC6 were coassociated proteins of both WDR76 and SPIN1, suggesting a potential role of SPIN1 in DDR as well.

To test whether SPIN1 also responds to DNA damage in live cells, we performed an imaging-based recruitment assay (2). In this assay, Halo- or SNAP-tagged proteins were expressed in HEK293 cells and labeled with the corresponding fluorescent ligands. Cells were also treated with Hoechst33258 as sensitizer. Then, we performed microirradiation treatment, in which we induced DNA damage in a defined area on each cell using a 405 nm laser. After microirradiation, the treated cell was recorded for up to 2 min (Fig. 4*B*). Using this assay, we have previously reported the recruitment of WDR76 and XRCC5 to the irradiated region (2). Consistent with these previous findings, we now observed that WDR76 and XRCC5 were recruited to the damaged region within 30 s (Fig. 4*C*). Similarly, SNAP-tagged SPIN1 was also rapidly enriched in the laser damaged region (Fig. 4 *C* and *D*). Although the detailed mechanisms remained unclear, this result supports the hypothesis that both WDR76 and SPIN1 are involved in DDR. Intriguingly, the recruitment of SPIN1 was nearly concurrent with WDR76 but obviously slower than XRCC5 (Fig. 4*C*). To compare the kinetics of recruitments, we performed nonlinear fitting for the average Rt values of each protein and estimated the rate of recruitment using the time taken to reach half of MaxRT ($t_{MaxRT/2}$) (*SI Appendix*, Fig. S8 and Dataset S6E). The measurements showed that there was only 0.7 s of difference between the $t_{MaxRT/2}$ of WDR76 and SPIN1, versus XRCC5 was about 4 s quicker than WDR76 to reach the half of its MaxRT. This result suggested that SPIN1 and WDR76 might be recruited to DNA damage site as a complex through interaction with the Ku complex. This is also consistent with our FCCS result, which suggested that WDR76 and SPIN1 in complex were mobile in the nucleus.

Modeling the Structure of the WDR76:SPIN1:Nucleosome Complex. From the AP-MS and XL-MS analyses on SCAP-purified WDR76 and SPIN1 complexes (Fig. 5), a large number of cross-links were found between SPIN1, WDR76, and histones that mapped to multiple locations on each protein and were consistent with an accessible H3K4me3 binding pocket on SPIN1 (Fig. 5*B*). We therefore sought to generate a larger model of the structure of the WDR76:SPIN1:Nucleosome complex. To do so, we performed integrative structural modeling using cross-links identified from the current study, along with atomic structures from the Protein Data Bank (PDB) (52) and Alphafold (53) (*SI Appendix*, Table S1 and Fig. 3*D*). Integrative modeling was performed with the Python Modeling interface of the IMP (https://integrativemodeling.org) (34, 35, 54). The modeling followed previously established protocols (33, 55). Integrative modeling of the WDR76:SPIN1:Nucleosome complex resulted in a single cluster of models (92% of 29550 models) with a model precision of 24 Å where model precision is defined as the average RMSD between the cluster centroid and models in the cluster (Fig. 6 *A* and *B* and *SI Appendix*, Fig. S9). The models satisfied all the cross-links to SPIN1 and WDR76.

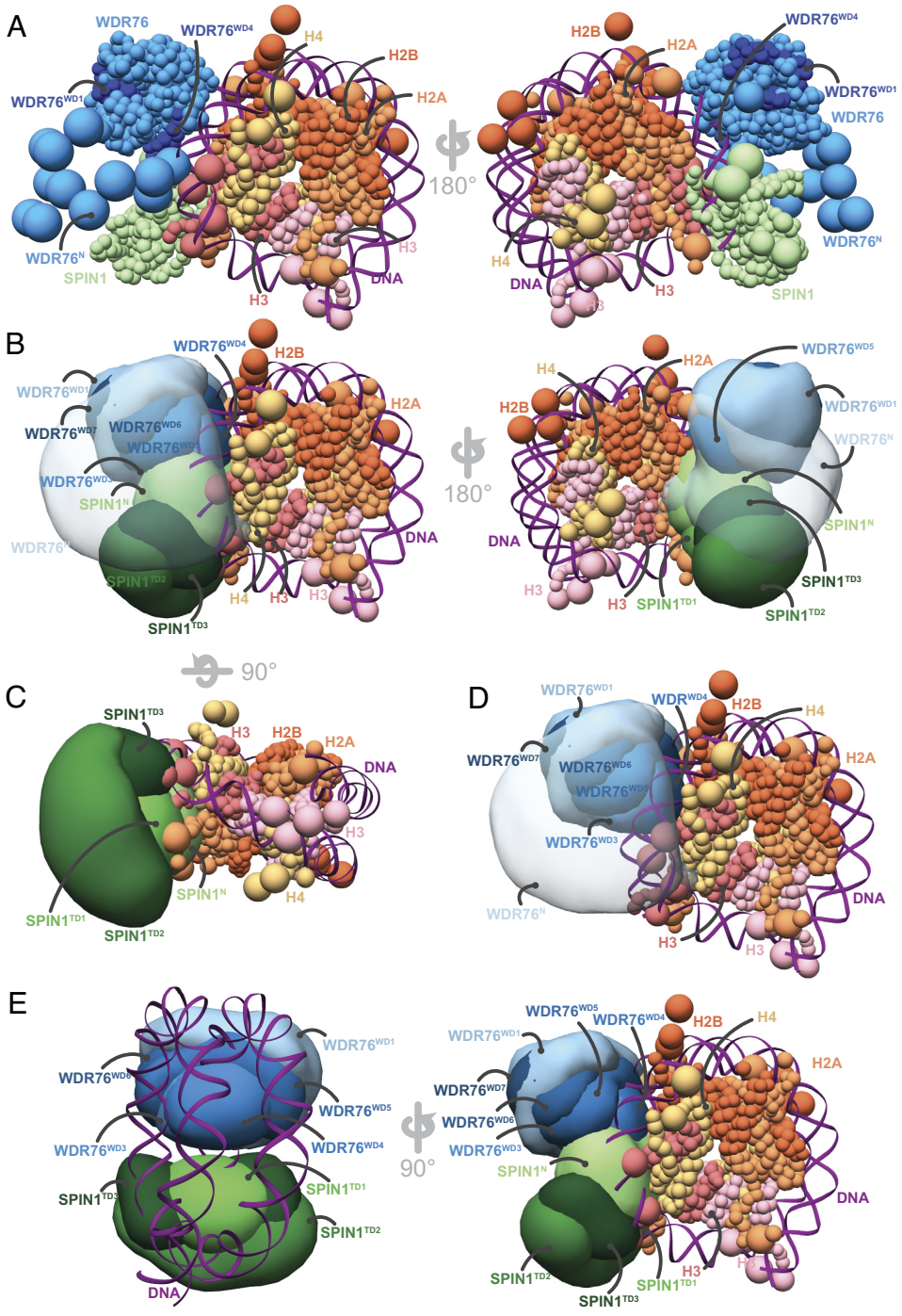

Fig. 6. Integrative structural model of the WDR76:SPIN1:Nucleosome complex. (*A*) Representative bead model from the most populated cluster of integrative structural models of the WDR76:SPIN1:Nucleosome complex. The model is colored by subunit. The two copies of H3 are shown in different shades of pink to better illustrate their interaction with SPIN1 and WDR76. DNA is shown in ribbon representation. WDR76^{WD1} and parts of WDR76^{WD4} are colored in a darker shade of blue to illustrate the looping of WDR76^{N}. (*B*) Localization probability density maps of the cluster showing the position of all domains/subunits. The domain densities are colored in progressively darker shades along the sequence for WDR76 and SPIN1. All maps are contoured at ~20% of their respective maximum voxel values. (*C*) Localization probability density map of SPIN1 domains with the nucleosome (WDR76 densities are hidden for clarity). (*D*) Localization probability density map of WDR76 domains with the nucleosome (SPIN1 densities are hidden for clarity). (*E*) Localization density maps from panel *B* (*Left*) turned by 90° along the *Y*-axis showing the WDR76–SPIN1 interaction. The nucleosome and the N-termini densities of both proteins are hidden for clarity. The interactions of SPIN1^{N} with nucleosome and WDR76 are shown (*Right*). See also *SI Appendix*, Figs. S9–S12 and Table S1.

In the overall architecture, SPIN1 and WDR76 are adjacent to each other on the same side of the nucleosome (Fig. 6 *A* and *B*). In the structures of SPIN1 and WDR76 in the complex, the SPIN1 Tudor1 domain (TD1) forms the core of SPIN1 and is surrounded by SPIN1 TD2 and TD3. SPIN1 TD2 is exposed, while other domains of SPIN1 are buried in this complex (Fig. 6 *B* and *C*). Next, WDR76 consists of a compact arrangement of the WD40 repeat domains (WD) in the canonical β-propeller structure. The N terminus of WDR76 (WDR76-N) extends from its central WD1 domain, flanking one side of the β-propeller, and looping back to the WD4 and WD5 domains (Fig. 6*A*). WDR76-N and WD1 are exposed, while other domains of WDR76 are buried (Fig. 6*B*).

SPIN1 and WDR76 interact where the N terminus of SPIN1 (SPIN1-N) and SPIN1 TD1 are proximal to WDR76-N and WDR76 WD3-WD5, while SPIN1 TD3 interacts with WDR76-N alone. The SPIN1–WDR76 interaction appears to be mostly mediated by their N-termini (Fig. 6 *B* and *E* and *SI Appendix*, Fig. S10).

SPIN1 and WDR76 both interact with the nucleosome. SPIN1-N and SPIN1 TD1 both interact with the N-terminal tail of histone H3 (H3-N), and the cores of H3 and H4 (Fig. 6 *B* and *C* and *SI Appendix*, Fig. S10). SPIN1-N additionally interacts with the core of H2A (Fig. 6*B* and *SI Appendix*, Fig. S10). Finally, SPIN1 TD3 interacts with H3-N alone (Fig. 6*C* and *SI Appendix*, Fig. S10). Moreover, the similarity of the SPIN1–H3 binding site in our model to that in PDB 4H75 (22) validates our integrative model since this information was not used as input. Next, the N terminus of WDR76 (WDR76-N), WDR76 WD3, and WD4 interact with H3-N and the core of H2A (Fig. 6 *B* and *D* and *SI Appendix*, Fig. S10). Additionally, WDR76-N interacts with H3 core and WD4 with H2B core (Fig. 6 *B* and *D* and *SI Appendix*, Fig. S10). This is consistent with previous AP-MS studies that show that WDR76 interacts with histones primarily through its N terminus (3). There are both low- and high-precision regions in this model. Based on precision analysis of our integrative models, the residues 245 to 251 in WDR76-N, SPIN1 TD1, and TD3, and the WDR76 WD domains are of high precision, SPIN1-N has a medium precision, and most of WDR76-N and the histone tails are of low precision (Fig. 6 *B–D* and *SI Appendix*, Fig. S11).

Discussion

WDR76 was first identified in yeast through AP-MS analysis of core histones (1). Its amino acid sequence contains seven WD40 domain repeats and is conserved in higher eukaryotes (3). Comprehensive AP-MS studies of human WDR76 identified many legitimate interactions (2, 3), yet its function remains enigmatic. One reason is that WDR76 might conduct various activities with different binding partners (Fig. 1*A*). This multiplicity is difficult to resolve by conventional AP-MS approaches but is a good test case to demonstrate the power of SCAP technology. Among the WDR76 copurified proteins, we chose SPIN1 as the other bait protein to perform SCAP. SPIN1 binds H3K4me3 with its second Tudor domain (22, 23); thus, its interaction with WDR76 inferred their collaborative function in chromatin related activities. Core histones appeared as major coassociated proteins of the WDR76:SPIN1 complex enriched by SCAP (Fig. 2*C*). In addition, SCAP successfully enriched 35 cocaptured proteins of both WDR76 and SPIN1 in the final elution after the second affinity step (E2 fraction) when compared to the first elution (E1 fraction).

SCAP-XL of WDR76 and SPIN1 provided evidence for direct protein–protein interactions (Fig. 3*D*). No cross-linking site was observed in the second Tudor domain of SPIN1 in this analysis (Fig. 3*D*), indicating that the interaction of SPIN1 with WDR76 might not prevent it from binding to H3K4me3. This is consistent with the conclusion from PTM analysis of histone H3 by SCAP coupled with mass spectrometry or Western blot (Fig. 3 *B* and *C*) that the WDR76:SPIN1 complex might selectively bind certain epigenetic markers where SPIN1 likely plays a primary role in this selectivity. As additional evidence, the H3K4me3 binding pocket of SPIN1 has no overlap with the interface with WDR76 in the model (Fig. 5*B*). Moreover, WDR76 was cross-linked to H3K4 and H3K9, which are likely to be modified in SPIN1-bound histone H3. This interesting observation suggests the possibility for WDR76 and SPIN1 in the complex bind two different copies of histone H3.

Another SPIN1-containing complex, SPIN1:SPINDOC, was previously analyzed using SCAP technology (32). The SCAP-MS results suggested that the complex SPIN1 formed with WDR76 is a different complex from the one formed with SPINDOC (Dataset S2D). In contrast to the WDR76:SPIN1 complex, SPIN1 lost binding of histone H3 in the SPIN1:SPINDOC complex (Fig. 3*C*). This is also supported by structural modeling results: In the SPIN1:SPINDOC complex, SPINDOC blocks the H3K4me3 binding pocket of SPIN1, whereas the pocket is left open in the WDR76:SPIN1 model (*SI Appendix*, Fig. S7). It is worth noting that in this study, we showed evidence of WDR76:SPIN1 being recruited to laser-induced DNA damage sites as a complex (Fig. 4). Intriguingly, work by Yang et al. (56) reported the recruitment of SPINDOC to DNA damage and its interaction with DDR protein, PARP1. PARP1 was also captured by SCAP for WDR76:SPIN1 (Fig. 4*A*). The recruitment of WDR76, SPIN1, and SPINDOC to DNA damages and their interactions with classic DDR proteins implies a potential model in which SPIN1 switches between complexes at the damaged site in coordination with other DDR proteins. Such a mechanism needs to be further investigated in future studies as well as whether the binding or releasing of histone marks by SPIN1 complexes is related to DDR.

Finally, given the cross-links found between WDR76, SPIN1, and histones, we were able to build an integrative structural model of WDR76:SPIN1 and docked to the nucleosome. There were several functional insights provided by this integrative structure. First, we observed that SPIN1 and WDR76 both interact simultaneously with the same H3 molecule. In most models in the ensemble, both SPIN1 and WDR76 interacted with only one H3 molecule (*SI Appendix*, Fig. S12 *A* and *B*). In our structure, SPIN1-N appeared to occupy the space between WDR76 (upper half) and the SPIN1 TD domains (lower half) next to the nucleosome (Fig. 6). In fact, SPIN1 is closer to the nucleosome than WDR76 (*SI Appendix*, Fig. S12*C*). Taken together, we propose the potential mechanism where SPIN1 recognizes target sites on a nucleosome through its Tudor domains and then, SPIN1-N recruits WDR76 to the nucleosome through WDR76-N.

The ability to isolate specific complexes from larger protein interaction networks is a key feature of the SCAP technology. From such an approach, one can then elucidate specific molecular features and functions of specific complexes. Here, we demonstrated that the WDR76:SPIN1 complex had distinct features and functions compared to the SPIN1:SPINDOC complex. A major distinction between these complexes was the ability of WDR76:SPIN1 to interact with histones and recognize the H3K4me3 modification, whereas SPIN1:SPINDOC does not. By then coupling the SCAP approach with XL-MS in the study of both complexes, we built integrated structural models demonstrating that while in the SPIN1:SPINDOC complex the H3K4me3 binding pocket of SPIN1 is buried, it is accessible in the WDR76:SPIN1 complex. XL-MS analyses confirmed the direct interaction between WDR76 and SPIN1, in addition to several cross-links between histones H2B, H3 and H4 with SPIN1 or WDR76 (Fig. 5*B*). Then, using the state-of-the-art IMP platform (33–35, 54, 55), we built an integrated structural model of WDR76:SPIN1 and the nucleosome (Fig. 6). This demonstrates that as long as any two proteins can have either the HaloTag or SNAP-tag integrated into their N- or C- termini coupling the SCAP technology with XL-MS and IMP, one can elucidate molecular and functional insights into specific protein complexes culminating with an integrative structural model of the complex.

Materials and Methods

Critical Reagents, Plasmids, and Cell Lines. The same critical reagents that are commercially available were provided in ref. 32. Sequences of WDR76, SPIN1, and XRCC5 open reading frame (ORF) were obtained from Kazusa Genome Technology (Kisarazu, Chiba, Japan). Vectors used for expressing Halo- or SNAP-tagged proteins, including the dual expression vector, were also described before in ref. 32. The WDR76 knockout cell line was derived from Flp-In™-293 Cell Line purchased from Invitrogen (Carlsbad, CA). The knockout was achieved using RNA-guided CRISPR-Cas9 system (57). Additional details in *SI Appendix*.

Single-Bait AP and SCAP. All purifications were performed using stable expression cell lines, except that blank control purifications were performed on cells without expression of tagged proteins. Halo purifications were performed according to the manual of HaloTag® Mammalian Pull-Down Systems (Promega, Madison, WI) except for cells were lysed with high salt buffer (20 mM Hepes at pH 7.9, 560 mM NaCl, 10 mM KCl, 1.5 mM MgCl2, 1% Triton® X-100, 1 mM Dithiothreitol, Salt Active Nucleases, and Protease Inhibitor Cocktail) at a 1:3 ratio by volume (final 420 mM NaCl). SCAP enrichment was performed as previously described using 293FRT cells stably expressing a pair of baits expressing either the SNAP or the Halo tag (32). For each type of purification, three replicates were performed. For comparing the pulldown of H3K4me3 by WDR76:SPIN1 and SPIN1:SPINDOC, SCAP was performed as previously described (32) with minor adjustments using Flp-In™-293 cells stably expressing Halo-WDR76/SNAP-SPIN1 or Halo-SPIN1/SNAP-SPINDOC. For purifications where acetylation was probed, sodium butyrate (1 mM) was added to all buffers to inhibit HDACs. Additional details are provided in *SI Appendix*.

Cross-Linking Analysis of Halo-WDR76 AP-XL and Halo-WDR76/SNAP-SPIN1 SCAP-XL. The cells used for Halo-WDR76 AP-XL were deleted of endogenous WDR76. For each purification, a cell pellet of approximately 0.5 mL was subjected to Halo purification. The Halo purification method was described in the specific method section above. Samples from four replicates were analyzed by mass spectrometry. The SCAP-XL of Halo-WDR76 and SNAP-SPIN1 were performed in two different scales, either with a cell pellet of ~1.5 mL or ~3 mL. The optimized SCAP protocol described in the previous method section was used in the SCAP-XL of Halo-WDR76/SNAP-SPIN1. For each scale, three replicates were performed. A total of six samples were analyzed by mass spectrometry. For cross-linking reactions, eluted copurified proteins from different purifications were cross-linked with 5 mM DSSO (disuccinimidyl sulfoxide) purchased from Thermo Fisher Scientific (Waltham, MA) at room temperature for 1 h. The cross-linking reaction was quenched by 50 mM Tris-HCl.

Mass Spectrometry Data Acquisition. For each sample, 5% of the amount processed for mass spectrometry analysis was loaded for sodium dodecyl-sulfate polyacrylamide gel electrophoresis (SDS-PAGE) and silver staining analysis first. Both not cross-linked and cross-linked samples were processed using the same procedures described previously (58). Each sample was first TCA precipitated and then resuspended with 8M Urea buffer (in 100 mM Tris-HCl, pH 8.5). The resuspended proteins were reduced with 5 mM tris(2-carboxyethyl)phosphine (TCEP) and treated with 10 mM 2-Chloroacetamide (CAM). Then, proteins were digested with Lys-C for at least 6 h followed by dilution to 2M urea and overnight trypsin digestion. Last, the digested samples were quenched with 5% formic acid. MudPIT has been described before (59) with additional details provided in *SI Appendix*. The LC-MS method for analyzing cross-linked samples has also been described before (32) with additional details provided in *SI Appendix*.

Cross-Linking Data Analysis. For the data analysis of DSSO cross-linked peptides, Proteome Discoverer 2.4 (Thermo Scientific, San Jose, CA) with add on XLinkX node was used in peptide identification and cross-linked peptide searching. The following settings were used: precursor ion mass tolerance, 10 ppm; fragment ion mass tolerance, 0.6 Da; fixed modification, Cys carbamidomethylation; variable modification, Met oxidation, Lys DSSO Amidated, and Lys DSSO hydrolyzed; maximum equal dynamic modification, 3. Proteins FDR was set at 0.01. Acetylation was selected as a dynamic modification. The raw files and search engine files for cross-linking datasets are available at MassIVE (Dataset S1A). The cross-linking results were visualized in 2D by a web-based software xiView (44) (https://xiview.org/xiNET_website/index.php). Tables uploaded to xiView can be found in Dataset S4.

Live Cell Imaging. As described previously, all cells used for imaging were plated into Mat-Tek dishes with No 1.5 coverslip bottoms. Imaging samples were kept in phenol red–free DMEM Medium with GlutaMAX and 10% FBS. While imaging, live cells are kept under 37 °C, 5% CO2, and humidified condition. For WDR76 and SPIN1 imaging experiments, pcDNA5FRT-SNAP-SPIN1 or pcDNA5FRT-SNAP were transfected to Halo-WDR76 stable expression cell line (with endogenous WDR76). For negative control experiments, pcDNA5FRT-SNAP was cotransfected with pcDNA5FRT-Halo to the original Flp-In™-293 Cell Line (Invitrogen); and for positive control experiments, pcDNA5FRT-Halo-NLS-SNAP was transfected. For the microirradiation assay, SNAP-tagged proteins were transiently expressed in Halo-WDR76 stable expression cell line (with endogenous WDR76). Cells were imaged 24 h after transfection. Halo tags were stained with HaloTag® Ligands TMRDirect (Promega), and SNAP tags were stained with SNAP-Cell® 505-Star (NEB). HaloTag® Ligands TMRDirect were added to medium to a final concentration of 50 nM and incubated overnight. SNAP-Cell® 505-Star ligands were added to medium at the same day of imaging, then cells were incubated with the ligands and washed. apFRET and FCCS were performed as described previously (32). For the microirradiation assay, HOECHST 33258 was also added together with SNAP ligands at a final concentration of 5 μg/mL. After staining, cells were allowed to stabilize in fresh medium for 30 min in the incubator before imaging. Additional details are provided in *SI Appendix*.

Structure Prediction and Integrative Complex Modeling. All 3D structures were visualized and manipulated by UCSF Chimera (60) to generate figures. Distances between the α-carbons of cross-linked lysine residues (Cα–Cα) were also measured in Chimera. For structure predictions, the full-length models of WDR76 (Uniprot: Q9H967) and SPIN1 (Uniprot: Q9Y657) were generated by I-Tasser (45, 46, 61) Online Server (https://zhanglab.ccmb.med.umich.edu/I--TASSER/) based on protein sequences. We next measured the distances between each pair of cross-linked lysine residues in every model (Dataset S5A). We allowed the maximum Cα–Cα distance of 35 Å between DSSO-cross-linked lysine residues to be considered satisfied. For WDR76 models, we found that both model3 and model5 were reasonably folded and satisfied 5 out of 6 intra-WDR76 cross-links (*SI Appendix*, Fig. S5*A*). For SPIN1, models are similar (*SI Appendix*, Fig. S5*B*); thus, we picked model2 as our best model for later analysis as it satisfied all seven intra-SPIN1 cross-links.

We next performed interaction space analysis using the quick scanning mode of DisVis (47, 48) (https://wenmr.science.uu.nl/disvis/). Either WDR76 model3 or model5 were used as the fixed chain and SPIN1 model2 was used as the scanning chain. The three cross-links detected between WDR76 and SPIN1 by SCAP-XL were used as restraints. For the analysis using WDR76 model3, no restraint was reported as false positive by DISVIS. For WDR76 model5, one restraint out of the 3 had a Z-score over 1 and suggested to be false positive by DISVIS (Dataset S5B). We therefore picked WDR76 model3 for the WDR76:SPIN1 complex modeling analysis. Molecular docking was performed using HADDOCK 2.4 webserver (49, 50) (https://wenmr.science.uu.nl/haddock2.4/). The docking was performed following HADDOCK tutorials and the protocol described by de Vries et al. (49) with additional details provided in *SI Appendix*.

Integrative Structural Modeling of the WDR76:SPIN1:Nucleosome Complex. The integrative structural modeling of the WDR76:SPIN1:Nucleosome complex was performed using the Integrative Modeling Platform (IMP 2.16.0) and its Python Modeling Interface (PMI) (34, 35, 54). The modeling pipeline in the current study is based on previously described protocols (33, 55, 62). The input data, scripts, and resulting integrative models of the Wdr76:Spin1:nucleosome complex are available at https://github.com/isblab/wdr76_spin1_nucleosome. The modeling proceeded in four stages.

The first stage involved gathering the necessary data. A 1:1:1 WDR76:SPIN1:nucleosome complex was modeled. The input data included 78 DSSO cross-links from SCAP-E2 tagged WDR76-SPIN1 and 13 cross-links from HALO-tagged WDR76 constructs from the current study, X-ray structures of $SPIN1^{45-259}$ (PDB 4H75) and the nucleosome (PDB 5GT0), and Alphafold structure of $WDR76^{245-276,\,288-626}$ (AF-19H967-F1, considering residues with reliable prediction, i.e., pLDDT greater than 70) (*SI Appendix*, Table S1) (22, 53, 63).

The second state involved representing the system and translating data into spatial restraints. Each protein was represented by a series of contiguous spherical beads along the backbone, each bead denoting a fixed number of residues.

Protein domains with known atomic structure (X-ray or Alphafold) were represented at 1 and 10 residues per bead and modeled as rigid bodies, whereas domains without known atomic structure (such as the WDR76-N) were modeled as flexible strings of beads at 20 (10) residues per bead for WDR76:SPIN1 (histones) (*SI Appendix*, Table S1). The Bayesian cross-linking restraint was used to restrain the relative distances of cross-linked residues. Excluded volume and connectivity restraints were included to enforce the correct stereochemistry (33).

The third stage involved structural sampling to produce an ensemble of structures that satisfies the restraints. The rigid bodies consisted of the WD domains of WDR76 and TD domains of SPIN1, whereas their unstructured termini and the histone tails comprised the flexible beads. The position of the nucleosome core was fixed throughout sampling. The Monte Carlo moves included random translations of individual beads in the flexible segments and random rotations and translations of rigid bodies and super rigid bodies. A model was saved every 10 Gibbs sampling steps, each consisting of a cycle of Monte Carlo steps that moved every bead and rigid body once. Starting with random initial configurations for the rigid bodies and flexible beads, 60 million models were sampled using Replica Exchange Gibbs Sampling Markov Chain Monte Carlo algorithm, under the cross-linking, excluded volume, and connectivity restraints.

The fourth stage involved analyzing and validating the ensemble of structures. First a sampling exhaustiveness, clustering, and precision analysis was conducted. The sampled models were filtered based on the restraint scores, followed by assessment of sampling exhaustiveness, structural clustering, estimation of model precision, and visualizing the variability in the ensemble of structures using localization probability density maps (*SI Appendix*, Fig. S8) (33, 55, 62). The localization probability density map for a protein domain specifies the probability of a voxel being occupied by a bead belonging to the domain in a set of superposed models. Regions of high- and low-precision were computed using PrISM and visualized on the cluster center bead model (*SI Appendix*, Fig. S11) (64). All models and densities were visualized with UCSF Chimera and ChimeraX (65).

Next, a fit to input data was carried out. The fit to cross-links was computed by obtaining the percentage of satisfied cross-links in the major cluster; a DSSO cross-link is satisfied if the corresponding Cα–Cα distance in any model in the cluster is less than 35 Å. The cluster generally satisfied the excluded volume and sequence connectivity restraints. This was followed by a fit to data not used in modeling. The integrative structure was validated by two pieces of information that were not used to compute the model. First, the SPIN1–H3 binding site in the structure is similar to that in the crystal structure of SPIN1–H3 complex (PDB 4H75) (22). Second, WDR76 interacts with histones through its N-termini, as seen in AP-MS studies (3). Next protein–protein distance maps were created to visualize interacting regions by computing the average distance between bead surfaces across all the models in the major cluster (*SI Appendix*, Fig. S7). The final analysis step determined which molecules of H3 interact with SPIN1 and WDR76 and which of SPIN1 and WDR76 is closer to H3. To accomplish this, the distance between the center of mass of the closest SPIN1 (or WDR76) domain and the center of mass of each H3 molecule was computed and visualized for each model in the major cluster (*SI Appendix*, Fig. S12).

Data, Materials, and Software Availability. The availability of mass spectrometry datasets in public repositories is provided in Dataset S1. Additional Data for the analysis and processing of all mass spectrometry data are provided in Datasets S2–S4. The data regarding the fluorescent imaging experiments are provided in Dataset S6. Original data underlying this manuscript generated at the Stowers Institute may be accessed after publication from the Stowers Original Data Repository at http://www.stowers.org/research/publications/libpb-1626 (66). Inputs for integrative modeling via IMP Modeling Platform inputs are provided in *SI Appendix*, Table S1. The set of input data, scripts, and resulting integrative models of the WDR76:SPIN1:nucleosome complex are publicly available at https://github.com/isblab/wdr76_spin1_nucleosome (67). The structures will also be available in the PDB-Dev repository (https://pdb-dev.wwpdb.org) under the ID PDBDEV_00000382 (68). Mass spectrometry data have been deposited in MASSIVE (MSV000086846 (69), MSV000086802 (70), MSV000086849 (71), MSV000086749 (72), MSV000086828 (73), and MSV000094548 (74)). All other data are included in the manuscript and/or supporting information.

ACKNOWLEDGMENTS. The research presented here was supported by the Stowers Institute for Medical Research, the National Institute of General Medical Sciences of the NIH grants T32GM138077 (J.C.), R35GM118068 (J.L.W.), and R35GM145240 (M.P.W.). Additional support was provided to S.V. from the Department of Atomic Energy, Government of India, through grant DAE TIFR RTI 4006 and from the Science Engineering and Research Board, Department of Science and Technology, Government of India grant SPG/2020/000475.

Author affiliations: [a]Stowers Institute for Medical Research, Kansas City, MO 64110; [b]Medical Scientist Training Program, Department of Cancer Biology, University of Kansas Medical Center, Kansas City, KS 66150; [c]National Centre for Biological Sciences, Tata Institute of Fundamental Research, Bangalore 560065, India; and [d]Department of Biochemistry and Molecular Biophysics, Washington University St. Louis School of Medicine, St. Louis, MO 63110

Author contributions: X.L., Y.Z., L.F., J.L.W., and M.P.W. designed research; X.L., Y.Z., Y.H., C.A.S.B., J.C., S.B., S.A., J.J.L., B.D.S., J.R.U., and S.V. performed research; X.L., C.A.S.B., J.C., S.B., S.A., J.J.L., Y.X., B.A.G., S.V., and L.F. contributed new reagents/analytic tools; X.L., Y.Z., Z.W., Y.H., J.C., S.B., S.A., B.D.S., J.R.U., S.V., L.F., J.L.W., and M.P.W. analyzed data; and X.L., J.C., S.B., S.A., S.V., L.F., J.L.W., and M.P.W. wrote the paper.

1. J. M. Gilmore *et al.*, Characterization of a highly conserved histone related protein, Ydl156w, and its functional associations using quantitative proteomic analyses. *Mol. Cell. Proteomics* **11**, M111.011544 (2012).
2. J. M. Gilmore *et al.*, WDR76 co-localizes with heterochromatin related proteins and rapidly responds to DNA damage. *PLoS One* **11**, e0155492 (2016).
3. G. Dayebgadoh, M. E. Sardiu, L. Florens, M. P. Washburn, Biochemical reduction of the topology of the diverse WDR76 protein interactome. *J. Proteome Res.* **18**, 3479–3491 (2019).
4. D. H. Choi, S. H. Kwon, J. H. Kim, S. H. Bae, Saccharomyces cerevisiae Cmr1 protein preferentially binds to UV-damaged DNA in vitro. *J. Microbiol.* **50**, 112–118 (2012).
5. J. M. Tkach *et al.*, Dissecting DNA damage response pathways by analysing protein localization and abundance changes during DNA replication stress. *Nat. Cell Biol.* **14**, 966–976 (2012).
6. I. Gallina *et al.*, Cmr1/WDR76 defines a nuclear genotoxic stress body linking genome integrity and protein quality control. *Nat. Commun.* **6**, 6533 (2015).
7. E. Y. Basenko, M. Kamei, L. Ji, R. J. Schmitz, Z. A. Lewis, The LSH/DDM1 homolog MUS-30 is required for genome stability, but not for DNA methylation in Neurospora crassa. *PLoS Genet.* **12**, e1005790 (2016).
8. B. D. Weger *et al.*, The light responsive transcriptome of the zebrafish: Function and regulation. *PLoS One* **6**, e17080 (2011).
9. J. W. Jones, P. Singh, C. K. Govind, Recruitment of Saccharomyces cerevisiae Cmr1/Ydl156w to coding regions promotes transcription genome wide. *PLoS One* **11**, e0148897 (2016).
10. Y. Jiang *et al.*, EGLN1/c-Myc induced lymphoid-specific helicase inhibits ferroptosis through lipid metabolic gene expression changes. *Theranostics* **7**, 3293–3305 (2017).
11. L. A. Higa *et al.*, CUL4-DDB1 ubiquitin ligase interacts with multiple WD40-repeat proteins and regulates histone methylation. *Nat. Cell Biol.* **8**, 1277–1283 (2006).
12. A. G. Tamayo, H. A. Duong, M. S. Robles, M. Mann, C. J. Weitz, Histone monoubiquitination by Clock-Bmal1 complex marks Per1 and Per2 genes for circadian feedback. *Nat. Struct. Mol. Biol.* **22**, 759–766 (2015).
13. W. J. Jeong *et al.*, WDR76 is a RAS binding protein that functions as a tumor suppressor via RAS degradation. *Nat. Commun.* **10**, 295 (2019).
14. E. J. Ro *et al.*, WDR76 degrades RAS and suppresses cancer stem cell activation in colorectal cancer. *Cell Commun. Signal.* **17**, 88 (2019).
15. J. C. Park, W. J. Jeong, S. H. Seo, K. Y. Choi, WDR76 mediates obesity and hepatic steatosis via HRas destabilization. *Sci. Rep.* **9**, 19676 (2019).
16. J. Yang, F. Wang, B. Chen, The role of WDR76 protein in human diseases. *Bosn. J. Basic Med. Sci.* **21**, 528–534 (2021).
17. Y. Hu, X. Tan, L. Zhang, X. Zhu, X. Wang, WDR76 regulates 5-fluorouracil sensitivity in colon cancer via HRAS. *Discov. Oncol.* **14**, 45 (2023).
18. M. Kwon *et al.*, Kurarinone induced p53-independent G0/G1 cell cycle arrest by degradation of K-RAS via WDR76 in human colorectal cancer cells. *Eur. J. Pharmacol.* **923**, 174938 (2022).
19. L. Fang, G. Yu, W. Yu, G. Chen, B. Ye, The correlation of WDR76 expression with survival outcomes and immune infiltrates in lung adenocarcinoma. *PeerJ* **9**, e12277 (2021).
20. T. Bartke *et al.*, Nucleosome-interacting proteins regulated by DNA and histone methylation. *Cell* **143**, 470–484 (2010).
21. Q. Zhao *et al.*, Structure of human spindlin1. Tandem tudor-like domains for cell cycle regulation. *J. Biol. Chem.* **282**, 647–656 (2007).
22. N. Yang *et al.*, Distinct mode of methylated lysine-4 of histone H3 recognition by tandem tudor-like domains of Spindlin1. *Proc. Natl. Acad. Sci. U.S.A.* **109**, 17954–17959 (2012).
23. X. Su *et al.*, Molecular basis underlying histone H3 lysine-arginine methylation pattern readout by Spin/Ssty repeats of Spindlin1. *Genes Dev.* **28**, 622–636 (2014).
24. J. X. Wang *et al.*, SPINDLIN1 promotes cancer cell proliferation through activation of WNT/TCF-4 signaling. *Mol. Cancer Res.* **10**, 326–335 (2012).
25. H. Franz *et al.*, The histone code reader SPIN1 controls RET signaling in liposarcoma. *Oncotarget* **6**, 4773–4789 (2015).
26. D. M. Janecki *et al.*, SPIN1 is a proto-oncogene and SPIN3 is a tumor suppressor in human seminoma. *Oncotarget* **9**, 32466–32477 (2018).
27. M. Lachner, D. O'Carroll, S. Rea, K. Mechtler, T. Jenuwein, Methylation of histone H3 lysine 9 creates a binding site for HP1 proteins. *Nature* **410**, 116–120 (2001).
28. M. Vermeulen *et al.*, Quantitative interaction proteomics and genome-wide profiling of epigenetic histone marks and their readers. *Cell* **142**, 967–980 (2010).
29. L. Kaustov *et al.*, Recognition and specificity determinants of the human cbx chromodomains. *J. Biol. Chem.* **286**, 521–529 (2011).

30. N. Bae *et al.*, A transcriptional coregulator, SPIN.DOC, attenuates the coactivator activity of Spindlin1. *J. Biol. Chem.* **292**, 20808–20817 (2017).
31. M. S. Devi *et al.*, Spindlin docking protein (SPIN.DOC) interaction with SPIN1 (a histone code reader) regulates Wnt signaling. *Biochem. Biophys. Res. Commun.* **511**, 498–503 (2019).
32. X. Liu *et al.*, Driving integrative structural modeling with serial capture affinity purification. *Proc. Natl. Acad. Sci. U.S.A.* **117**, 31861–31870 (2020), 10.1073/pnas.2007931117.
33. S. Arvindekar *et al.*, Molecular architecture of nucleosome remodeling and deacetylase sub-complexes by integrative structure determination. *Protein Sci.* **31**, e4387 (2022).
34. M. P. Rout, A. Sali, Principles for integrative structural biology studies. *Cell* **177**, 1384–1403 (2019).
35. D. Russel *et al.*, Putting the pieces together: Integrative modeling platform software for structure determination of macromolecular assemblies. *PLoS Biol.* **10**, e1001244 (2012).
36. D. Saltzberg *et al.*, Modeling biological complexes using integrative modeling platform. *Methods Mol. Biol.* **2022**, 353–377 (2019).
37. A. L. Olins, G. Rhodes, D. B. Welch, M. Zwerger, D. E. Olins, Lamin B receptor: Multi-tasking at the nuclear envelope. *Nucleus* **1**, 53–70 (2010).
38. G. V. Los, K. Wood, The HaloTag: A novel technology for cell imaging and protein analysis. *Methods Mol. Biol.* **356**, 195–208 (2007).
39. A. Keppler *et al.*, A general method for the covalent labeling of fusion proteins with small molecules in vivo. *Nat. Biotechnol.* **21**, 86–89 (2003).
40. Y. Sun, C. Rombola, V. Jyothikumar, A. Periasamy, Forster resonance energy transfer microscopy and spectroscopy for localizing protein–protein interactions in living cells. *Cytometry A* **83**, 780–793 (2013).
41. K. Bacia, S. A. Kim, P. Schwille, Fluorescence cross-correlation spectroscopy in living cells. *Nat. Methods* **3**, 83–89 (2006).
42. D. A. Wolters, M. P. Washburn, J. R. Yates III, An automated multidimensional protein identification technology for shotgun proteomics. *Anal. Chem.* **73**, 5683–5690 (2001).
43. H. Choi, D. Fermin, A. I. Nesvizhskii, Significance analysis of spectral count data in label-free shotgun proteomics. *Mol. Cell. Proteomics* **7**, 2373–2385 (2008).
44. M. Graham, C. Combe, L. Kolbowski, J. Rappsilber, xiView: A common platform for the downstream analysis of crosslinking mass spectrometry data. bioRxiv [Preprint] (2019). https://doi.org/10.1101/561829 (Accessed 26 February 2019).
45. Y. Zhang, I-TASSER server for protein 3D structure prediction. *BMC Bioinformatics* **9**, 40 (2008).
46. J. Yang *et al.*, The I-TASSER suite: Protein structure and function prediction. *Nat. Methods* **12**, 7–8 (2015).
47. G. C. van Zundert, A. M. Bonvin, DisVis: Quantifying and visualizing accessible interaction space of distance-restrained biomolecular complexes. *Bioinformatics* **31**, 3222–3224 (2015).
48. G. C. van Zundert *et al.*, The DisVis and PowerFit web servers: Explorative and integrative modeling of biomolecular complexes. *J. Mol. Biol.* **429**, 399–407 (2017).
49. S. J. de Vries, M. van Dijk, A. M. Bonvin, The HADDOCK web server for data-driven biomolecular docking. *Nat. Protoc.* **5**, 883–897 (2010).
50. G. C. P. van Zundert *et al.*, The HADDOCK2.2 web server: User-friendly integrative modeling of biomolecular complexes. *J. Mol. Biol.* **428**, 720–725 (2016).
51. H. H. Y. Chang, N. R. Pannunzio, N. Adachi, M. R. Lieber, Non-homologous DNA end joining and alternative pathways to double-strand break repair. *Nat. Rev. Mol. Cell Biol.* **18**, 495–506 (2017).
52. S. Bittrich *et al.*, RCSB protein data bank: Efficient searching and simultaneous access to one million computed structure models alongside the PDB structures enabled by architectural advances. *J. Mol. Biol.* **435**, 167994 (2023).
53. J. Jumper *et al.*, Highly accurate protein structure prediction with AlphaFold. *Nature* **596**, 583–589 (2021).
54. F. Alber *et al.*, Determining the architectures of macromolecular assemblies. *Nature* **450**, 683–694 (2007).
55. D. J. Saltzberg *et al.*, Using integrative modeling platform to compute, validate, and archive a model of a protein complex structure. *Protein Sci.* **30**, 250–261 (2021).
56. F. Yang *et al.*, SPINDOC binds PARP1 to facilitate PARylation. *Nat. commun.* **12**, 6362 (2021).
57. F. A. Ran *et al.*, Genome engineering using the CRISPR-Cas9 system. *Nat. Protoc.* **8**, 2281–2308 (2013).
58. S. K. Swanson, L. Florens, M. P. Washburn, Generation and analysis of multidimensional protein identification technology datasets. *Methods Mol. Biol.* **492**, 1–20 (2009).
59. L. Florens *et al.*, Analyzing chromatin remodeling complexes using shotgun proteomics and normalized spectral abundance factors. *Methods* **40**, 303–311 (2006).
60. E. F. Pettersen *et al.*, UCSF Chimera–A visualization system for exploratory research and analysis. *J. Comput. Chem.* **25**, 1605–1612 (2004).
61. A. Roy, A. Kucukural, Y. Zhang, I-TASSER: A unified platform for automated protein structure and function prediction. *Nat. Protoc.* **5**, 725–738 (2010).
62. S. Viswanath, I. E. Chemmama, P. Cimermancic, A. Sali, Assessing exhaustiveness of stochastic sampling for integrative modeling of macromolecular structures. *Biophys. J.* **113**, 2344–2353 (2017).
63. S. Padavattan *et al.*, Structural analyses of the nucleosome complexes with human testis-specific histone variants, hTh2a and hTh2b. *Biophys. Chem.* **221**, 41–48 (2017).
64. V. Ullanat, N. Kasukurthi, S. Viswanath, PrISM: Precision for integrative structural models. *Bioinformatics* **38**, 3837–3839 (2022).
65. E. F. Pettersen *et al.*, UCSF ChimeraX: Structure visualization for researchers, educators, and developers. *Protein Sci.* **30**, 70–82 (2021).
66. X. Liu *et al.*, SIMR-ODR. Stowers Institute. http://www.stowers.org/research/publications/libpb-1626. Deposited 18 July 2024.
67. S. Arvindekar *et al.*, Integrative model of the WDR76-SPIN1-Nucleosome complex. GitHub. https://github.com/isblab/wdr76_spin1_nucleosome. Deposited 12 September 2023.
68. S. Arvindekar *et al.*, Integrative model of the WDR76-SPIN1-Nucleosome complex. PDBDev. https://pdb-dev.wwpdb.org/entry.html?PDBDEV_00000382. Deposited 15 May 2024.
69. X. Liu *et al.*, Halo-Control/WDR76/SPIN1/CBX5_purification_MudPIT_wPTMs. MassIVE. https://doi.org/doi:10.25345/C5S50C. Deposited 11 February 2021.
70. X. Liu *et al.*, WDR76-SPIN1_inWDR76KO_SCAP-MS_MudPIT. MassIVE. https://doi.org/doi:10.25345/C5B79F. Deposited 3 February 2021.
71. X. Liu *et al.*, Halo-WDR76_Purification_WDR76KObackground_MudPIT_wPTMs. MassIVE. https://doi.org/doi:10.25345/C5CZ1Z. Deposited 11 February 2021.
72. X. Liu *et al.*, WDR76-SPIN1_SCAP-E2-XL_mzTab and mgf. MassIVE. https://doi.org/doi:10.25345/C55V3T. Deposited 22 January 2021.
73. X. Liu *et al.*, Halo-WDR76_Purification_inWDR76KO_DSSO-XL-MS. MassIVE. https://doi.org/doi:10.25345/C53J67. Deposited 9 February 2021.
74. X. Liu *et al.*, WDR76_SPIN1_Halo-AP_Enriched_Histones_AscendDIA. MassIVE. https://doi.org/doi:10.25345/C5M32NN1R. Deposited 15 April 2024.